Journal of the European Ceramic Society 21 (2001) 2221–2228

www.elsevier.com/locate/jeurceramsoc

Densification, microstructure and grain growth in the CeO_2–Fe_2O_3 system ($0 \leqslant Fe/Ce \leqslant 20\%$)

Tianshu Zhang [a,*], Peter Hing [a], Haitao Huang [a], J. Kilner [b]

[a] *Advanced Materials Research Centre, School of Materials Engineering, Nanyang Technological University, Nanyang Avenue, Singapore 636768, Singapore*

[b] *Department of Materials, Imperial College of Science, Technology and Medicine, London SW7 2AZ, UK*

Received 15 June 2000; received in revised form 8 November 2000; accepted 14 November 2000

Abstract

Mixtures of CeO_2 and Fe_2O_3 with Fe/Ce atomic ratios ranging from 0 to 0.2 were prepared by the conventional mixed-oxide technique. Small amount of Fe doping ($Fe/Ce \leqslant 1\%$) significantly promotes the densification and grain growth of CeO_2 ceramic. The results from the dilatometric measurement and SEM (scanning electronic microscopy) observation reveal that 0.5% Fe doping reduces the sintering temperatures by at least 200°C. For the samples with a large amount of Fe_2O_3 ($Fe/Ce \geqslant 1\%$), however, above 1400°C the densification behavior deteriorates remarkably; the density decreases with increasing sintering temperatures due to appearance of a lot of microcracks along grain boundaries. The so-called pining effect of second phase starts to take effect in the samples with Fe content greater than 5%. Fe_2O_3 grains grow more quickly at a lower sintering temperature ($\leqslant 1050$°C), compared with those of CeO_2.

Keywords: CeO_2–Fe_2O_3; Composites; Grain growth; Microstructure-final; Sintering

1. Introduction

Ceramic matrix composites have been made traditionally to improve micromechanics and mechanical behavior of some structural ceramics, such as Al_2O_3, SiC and Si_3N_4 and so on.[1] In the last 20 years, however, composite electroceramics have been extensively investigated and have found a wide application as resistors, sensors and transducers. Many properties of a two-phase mixture can be easily tailored by simply adjusting mixing ratios and microstructure. For example, hot pressed cristobalite-silicon carbide composite[2] and ZnO–NiO mixtures[3,4] exhibit a positive temperature coefficient of resistivity, while the single phase of these materials displays a negative temperature coefficient of resistivity. Park et al.[5] studied yttria stabilized zirconia (ionic)–NiO (electronic) mixtures, which are potential electrode materials for solid oxide fuel cells. They measured the electrical conductivity and electronic transference number of the mixture, and observed, with increasing NiO content a successive transition of conduction mechanism from ionic to mixed, and finally to electronic. More recently, Kim et al.[6] reported the electrical properties of the composite of 8 mol% Y_2O_3 stabilized zirconia (8% YSZ) and Mn_2O_3. This composite is a mixed ionic-electronic conductor, which has the potential uses as electrodes, electrocatalytic reactors and gas separation membrances. The entire composition range in the 8% YSZ–Mn_2O_3 system was divided into three regions based on activation energy and transference number.

In the present work, we focus on only the sintering and grain growth of the CeO_2–Fe_2O_3 system ($0 \leqslant Fe/Ce \leqslant 20\%$). A serial study on the electrical properties of this system is under way. Cerium (IV) oxide (CeO_2) is a very useful base material as catalyst supports, ion conductors and gas sensors. It is well known, however, that ceria based materials are difficult to densify below 1500°C.[7,8] In order to reduce the sintering temperatures, much attention has been paid to preparation of ultrafine CeO_2 powders by chemical and physical methods.[9–12] For the large-scale industrial application, however, it is useful to improve the sinterability of commercial CeO_2 powder by using sintering promoters.

Iron (III) oxide (Fe_2O_3) has two modifications, i.e. the γ-type with spinel structure and the α-type with corundum structure. We chose α-Fe_2O_3 as the electronic component for the mixed conducting composites, because α-Fe_2O_3 is

* Corresponding author. Tel.: +65-790-4614; fax: +65-793-5279.
E-mail address: p142713729@ntu.edu.sg (T. Zhang).

0955-2219/01/$- see front matter
PII: S0955-2219(00)00342-3

stable over a wide range of temperatures, and may promote densification of CeO_2 ceramic due to the effect of severely undersized dopants.[13] Moreover, from the periodic properties of elements, Fe element is a neighbor of Mn and Ni, and α-Fe_2O_3 exhibits good gas-sensing and catalystical properties.

Based on the literature reports,[14,15] we know that the solubility of Fe^{3+} into CeO_2 is small (less than 1.0% atomic ratio) in the range of room temperature to 1500°C. For clarity, our experimental results are reported by two subsections: one for the samples with Fe/Ce atomic ratios less than 1% (which can be treated as the single phase); the other for the samples with Fe/Ce atomic ratios ranging from 1 to 20% (which can be treated as a two-phase composite).

2. Experimental procedure

2.1. Preparation of samples

Fe-doped CeO_2 powders with atomic ratios of Fe/Ce ranging from 0 to 20% were prepared by the conventional mixed-oxide method from CeO_2 (>99.9% of purity) and Fe_2O_3 (>99.0% of purity). Both oxide powders have approximately the same average particle size of ~0.4 μm according to SEM observation and were dried at 150°C for 12 h before weighing. The powders were ground in ethanol by ball-milling using polypropylene jars with yttria-stabilized zirconia balls for over 24 h. After drying, the samples were pressed at ~50 MPa into pellets using a stainless steel die with 10 mm in diameter. Green densities are ~60% of theoretical.

2.2. Sintering experiment

The samples were heated up to a desired temperature in a furnace in air at a heating rate of 15 K/min and then held at this temperature for 1–5 h. The samples were naturally cooled to room temperature. Some sintering studies were performed in a vertical dilatometer (Model: Setsys 16/18, Setaram, France) in air with a constant heating rate (CHR). The dilatometer allowed continuous monitoring of the axial shrinkage. During the CHR experiments, the sample was heated at a constant rate of 10 K/min to the desired temperature and then cooled to room temperature.

The isotropic shrinkage of the sample was confirmed by measuring the radial and axial shrinkage. The time-dependent density, ρ, therefore, was calculated from the following equation:[16]

$$\rho = \left(\frac{L_f}{L_t}\right)^3 \rho_f \quad (1)$$

where L_f is the final length of the sample, L_t is the time-dependent length equal to the value of (L_0–ΔL_t) (L_0 is the original length of the sample and ΔL_t is the displacement of the sample at a certain time, t) and ρ_f is the final density obtained from the mass and dimension of the sample.

2.3. characterization of samples

The phase identification of samples was performed using X-ray diffraction (XRD) (Model: XRD-600, Shimadzu, Kyoto, Japan) with CuK_α radiation. Densities of sintered pellets were measured using both the Archimede method with water and calculation from the mass and the dimensions of the samples. It was found that both methods gave almost the same value. Microstructures of the samples, i.e. fracture surface or/and well-polished surface after thermal etching, was observed using scanning electron microscopy (SEM) (Model: JSM-5410. Oxford, UK). The distribution of iron element was detected using energy dispersive X-ray analysis spectroscopy (EDS). Grain sizes were measured from SEM micrographs of the etched samples by the linear intercept technique described by Mendelson.[17] The average crystallite size, D, was obtained as follows: $D = 1.56\ L$, where L is the average grain-boundary intercept length of a series of random lines on the SEM micrographs.

3. Results and discussion

3.1. CeO_2 doped with a small amount of Fe_2O_3 ($0 \leqslant Fe/Ce \leqslant 1\%$)

Due to the isotropic shrinkage of samples, the relative density (R.D.) as a function of temperature for different Fe contents can be calculated according to Eq. (1) and is shown in Fig. 1. The sintering curves for CeO_2 doped with more than 0.5% Fe nearly identical to that of 0.5% Fe-doped sample, for clarity, were omitted. In the temperature range used (i.e. room temperature to 1550°C), the density of pure CeO_2 increases with increasing temperature. Pure CeO_2 has only about 92% R.D. at 1550°C. This sintering behavior is very similar to the results reported by Zhou.[18] However, upon adding Fe_2O_3 into CeO_2, the sintering behavior changes greatly. The sample with 0.5% Fe doping has ~92% R.D. at ~1280°C, and reaches almost full densification (>99.0% R.D.) at 1400°C.

Fig. 2 shows densification rate $(1/\rho)$ $(d\rho/dt)$, as a function of temperature for the samples with different Fe contents. It is observed that with an increase in Fe content there is an obvious decrease in the temperature of maximum densification rate (T_{Max}). For example, T_{Max} changes from 1430°C for pure CeO_2 to 1225°C for 0.5% Fe doping. The difference in the values of T_{Max} for both samples is more than 200°C. The result suggests that Fe doping reduces the sintering temperatures

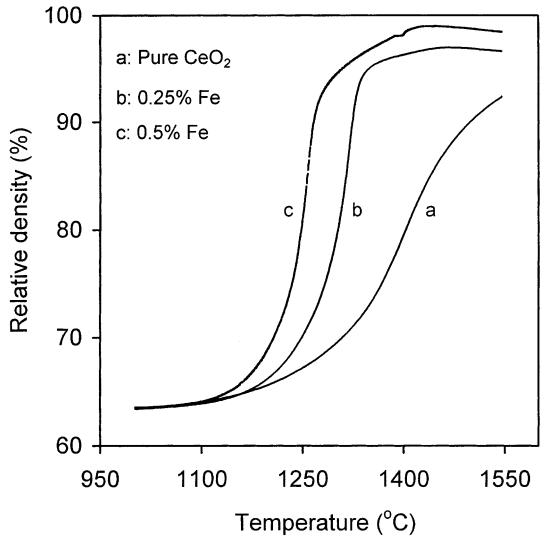

Fig. 1. Relative density vs temperature for (a) pure CeO_2, (b) 0.25% and (c) 0.5% Fe-doped CeO_2 at a heating rate of 10 K/min.

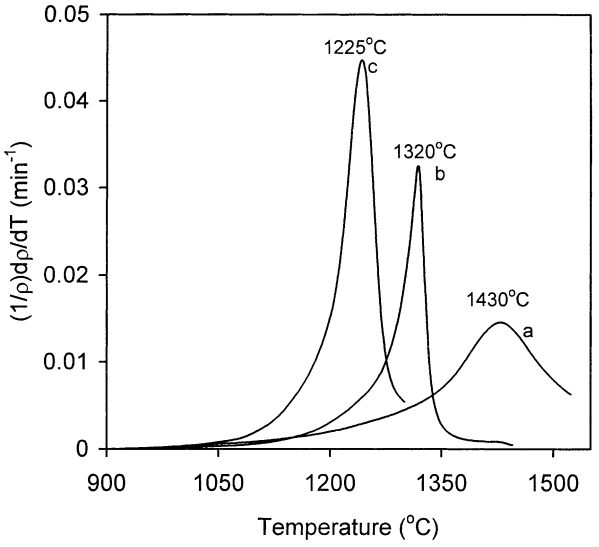

Fig. 2. Densification rate against sintering temperature for (a) pure CeO_2, (b) 0.25% and (c) 0.5% Fe-doped CeO_2.

dramatically. This reduction in the value of T_{Max} takes place mainly in the samples with Fe content ranging from 0 to 0.5%. No significant shift of T_{Max} towards lower temperature region can be observed in Fe content range greater than 0.5%. For clarity, only three curves of pure CeO_2, 0.25 and 0.5% Fe doping are shown in Fig. 2. It can be seen from this figure, on the other hand, that the densification rate increases significantly with Fe doping.

Selected microstructures of undoped, 0.5, and 1% Fe-doped CeO_2 sintered at 1300°C and 1500°C for 1 h are shown in Fig. 3(a)–(f), respectively. As shown in Fig. 3 (a), undoped CeO_2 ceramic sintered at 1300°C for 1 h is very porous (~82% R.D.), the grain size is ~0.6 μm, which is slightly larger than that of raw powder (~0.4 μm). However, the sample with 0.5% Fe doping sintered at the same conditions has a bigger crystallite size (~6.4 μm and reaches over 99.0% of relative density [Fig. 3(c)]. Moreover, it can be seen that 0.5% Fe-doped sample sintered at 1300°C [Fig. 3(c)] is much denser and exhibits a bigger grain size than that of pure CeO_2 sintered at 1500°C [Fig. 3(b)]. This result confirms that a small amount of Fe doping reduces the sintering temperatures by at least 200°C, which is in good agreement with that obtained from the dilatometer measurement. The darker grains shown in Fig. 3(c) and (e) by arrows are Fe_2O_3 as confirmed by EDS analysis.

Fig. 4(a) and (b) shows the effect of sintering temperatures on density and grain size for the samples with Fe/Ce = 0, 0.5 and 1% sintered at 900–1670°C for 1 h, respectively. The curves of relative density versus temperature below 1400°C for 0.5 and 1% Fe-doped samples show almost the same change trend [Fig. 4(a)]. In the temperature ranging from 1400 to 1670°C, the density of 0.5% Fe-doped sample shows a slight increase up to 1670°C, while that of 1% Fe-doped sample decreases from ~99.2% R.D. at 1400°C to ~90% R.D. at 1670°C. By examining the microstructure of 1% Fe-doped samples sintered above 1400°C as shown in Fig. 3(f), it is easy to understand that this decrease in density is due to the appearance of lots of microcracks along grain boundary, which leads to an expansion of the samples, thus gives a lower relative density. This phenomenon becomes severe with increasing both Fe/Ce atomic ratios and sintering temperatures. The density of pure CeO_2 increases as the sintering temperature increases, it reaches ~98.7% R.D. at 1670°C. From the morphology of fracture surface for undoped and 0.5% Fe-doped samples sintered at 1670°C for 1 h, we can find microcracks along grain boundary and holes in triple point junctions for pure CeO_2 ceramic, while none of these flaws can be found in 0.5% Fe-doped sample. These flaws lead to a slow densification of pure CeO_2 during final-stage sintering. It is observed from Fig. 4(b), on the other hand, that 0.5 and 1% Fe-doped samples have almost the same grain growth trend; a rapid grain growth starts above 1300°C, which corresponds to over 99.0% R.D. (~6.3 μm in grain size). It means that the densification is almost complete below 1300°C for both doped samples. Further increase in temperatures leads to only grain growth. For example, the grain size increases from ~6.3 μm at 1300°C for both to ~68.6 μm for 0.5% Fe doping and ~78.2 μm for 1% Fe doping at 1670°C. In addition, it seems that the microcracks along grain boundary in 1% Fe-doped sample have no effect on the grain growth.

Pure CeO_2 exhibits a rapid grain growth above 1500°C, in which it has ~95% R.D. (3.9 μm in grain size). Unlike the densification behavior of Fe-doped samples in the 1300 to 1670°C region as shown in Fig. 4(a) and (b),

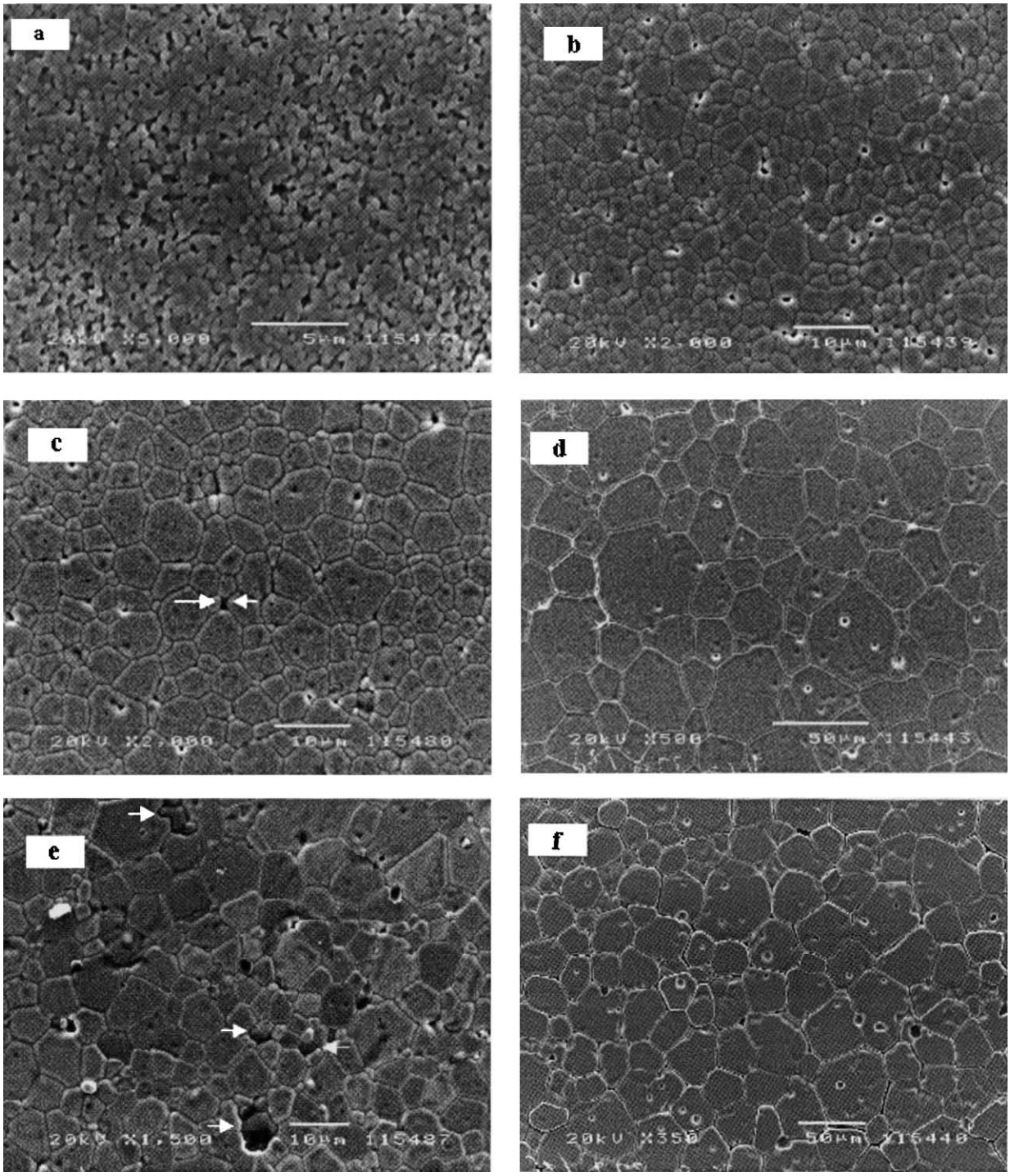

Fig. 3. SEM micrographs of undoped, 0.5 and 1% Fe-doped CeO_2 sintered at 1300 and 1500°C for 1 h, respectively: [1300°C: (a) pure CeO_2, (c) 0.5% Fe doping, (e) 1% Fe doping; and 1500°C: (b) pure CeO_2, (d) 0.5% Fe doping, (f) 1% Fe doping].

both the grain size and density of pure CeO_2 keep increasing as the temperature increases from 1500 to 1670°C. Moreover, the grain size of pure CeO_2 sintered at 1670°C is ~30 μm. This is just half the grain size of Fe-doped samples sintered at the same condition. Such these big differences between pure CeO_2 and Fe-doped CeO_2 are due to two main reasons:

1. The early-stage sintering mechanisms for doped and undoped samples are completely different. In our another report,[19] we confirmed that pure CeO_2 exhibited volume diffusion-controlled sintering, which dominated the densification up to 78% R.D., while 0.5% Fe-doped sample exhibited viscous flow, which dominated the densification up to 87% R.D.

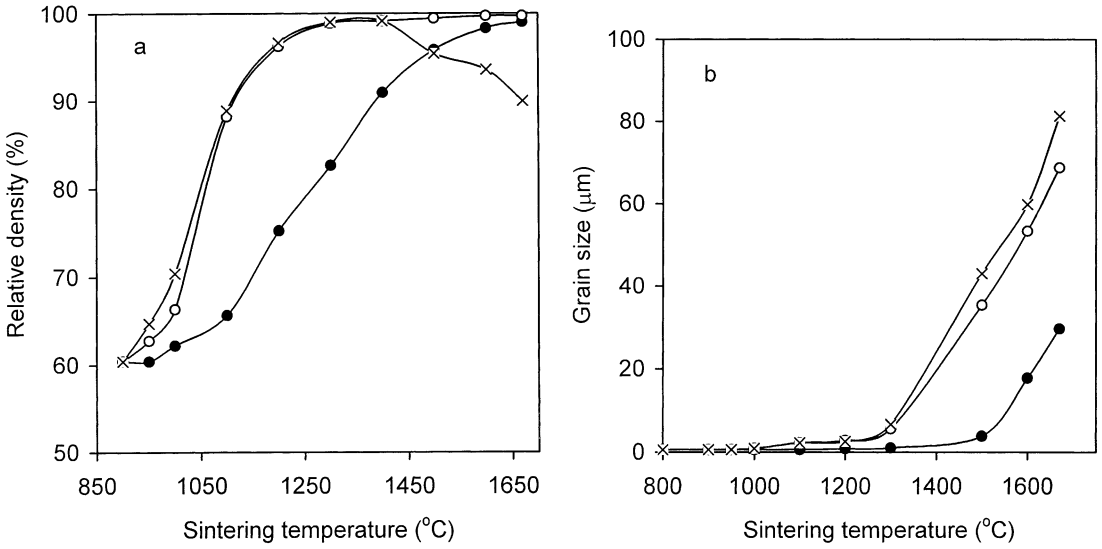

Fig. 4. Effect of sintering temperature on (a) relative density and (b) grain size of the samples doped with (●) 0, (○) 0.5 and (×) 1% Fe.

Furthermore, the sintering temperatures to achieve the above-mentioned densities, i.e. 78% and 87% R.D., were 1430°C for pure CeO_2 and 1225°C for 0.5% Fe-doped sample, respectively. A rapid densification rate of Fe-doped sample in the lower temperature range increases the contact area of particles in a compact, which will promote the diffusivity rate of matrix and thus enhances the grain growth.

2. The size (0.67 Å) of Fe^{3+} ion is severely undersized, compared with that (0.97 Å) of Ce^{4+} ion. Based on the report by Chen and Chen,[13] Fe^{3+} ions have a tendency to enhance grain boundary mobility, probably due to the large distortion of the surrounding lattice that facilitates defect migration.

3.2. CeO_2 mixed with a large amount of Fe_2O_3 ($1 \leqslant Fe/Ce \leqslant 20\%$)

The results from XRD analysis indicate that under the present experimental conditions no binary compounds, such as $FeCe_2O_4$ and $FeCeO_3$, can be formed in the CeO_2–Fe_2O_3 system. As stated before, the samples with $Fe/Ce \geqslant 1\%$ can be treated as a two-phase composite due to the solubility of small amount of Fe^{3+} in CeO_2 crystallites. In addition, the densification behavior deteriorates remarkably for the samples with $Fe/Ce \geqslant 1\%$ sintered above 1400°C. In this section, therefore, we concentrate on only the sintering behavior of the samples sintered below 1400°C. Fig. 5 shows SEM micrographs of the samples with $Fe/Ce = 3$ and 15% sintered at 1350°C for 5 h. Compared with micrographs of the samples doped with $Fe/Ce \leqslant 1\%$ as shown in Fig. 3(a) and (e), we can see that the number and size of Fe_2O_3 grains increase with increasing Fe content. For the samples with $Fe/Ce \geqslant 10\%$, most of Fe_2O_3 grains grow more rapidly than those of CeO_2 as shown in Fig. 5(b).

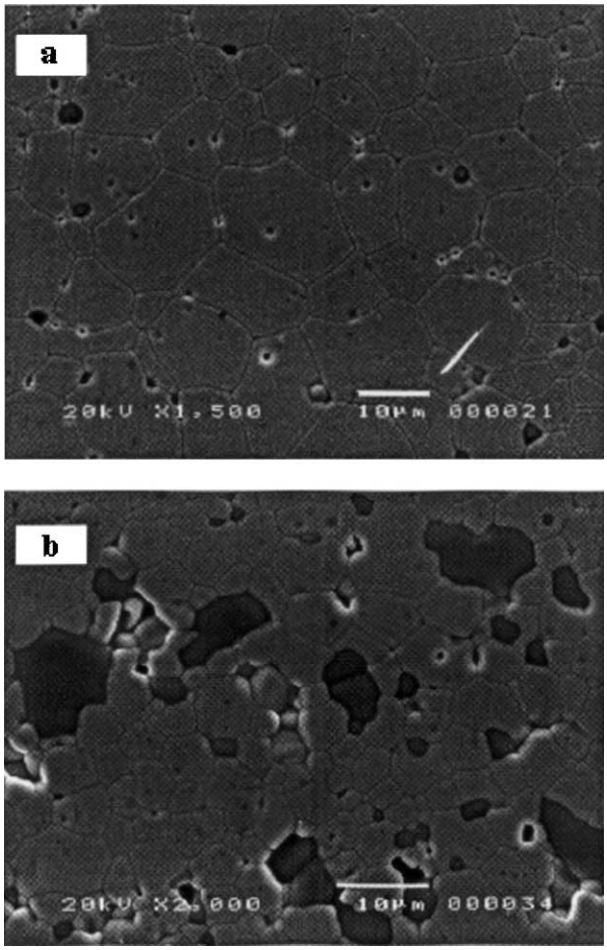

Fig. 5. SEM micrographs of the samples with (a) $Fe/Ce = 3$ and (b) 15% sintered at 1350°C for 5 h (dark grains are α-Fe_2O_3).

In order to clarify the densification of the two-phase composites, i.e. CeO_2 and Fe_2O_3, we studied the grain growth and microstructure of the samples with Fe/

Ce = 3 and 15% sintered at 1050–1350°C. Fig. 6 shows the effect of sintering temperature on the grain sizes of Fe_2O_3 and CeO_2 in the sample with Fe/Ce = 15%. The average grain sizes for both constituents keep increasing simultaneously. However, at 1050°C α-Fe_2O_3 has a bigger grain size (> 1 μm) than that (~0.4 μm) of CeO_2. It means that Fe_2O_3 grains grow fast even at a lower sintering temperature, which is closely connected with the nature of Fe_2O_3. Bonnet et al.[20] studied the sintering of the SnO_2–CuO system, and observed that the diffusion of copper ions on SnO_2 grains occurred during the previous calcination treatment at 400°C. Gouvea et al.[21] observed the segregation of MnO_2 on SnO_2 grains during the sintering of MnO_2-doped SnO_2. From the periodical properties of elements, Fe element should have similar property to that of the above-mentioned two elements (i.e. Mn and Cu). It is reasonable to assume, therefore, that Fe ions are easy to be dispersed onto CeO_2 grains at a lower sintering temperature (e.g. ~500–700°C); at a slightly higher sintering temperature which is far less than 1050°C, Fe^{3+} ions will nucleate and grow into bigger grains because well-dispersed Fe^{3+} ions on CeO_2 grains have an easy mass transportation channel (i.e. along grain boundary of CeO_2). This may be used to explain why Fe_2O_3 grains grow fast at a lower sintering temperature, although further study is still needed. The effect of Fe content on CeO_2 grain growth was also investigated in this study, and this is presented bellow. In addition, it seems that Fe_2O_3 distribution in Fig. 5(b) is very inhomogenous. As a mater of fact, it is due to this micrograph with a large magnification. By observing the micrographs with a small magnification as shown in Fig. 7, we can see that the distribution of Fe_2O_3 grains in CeO_2 matrix is random and homogenous.

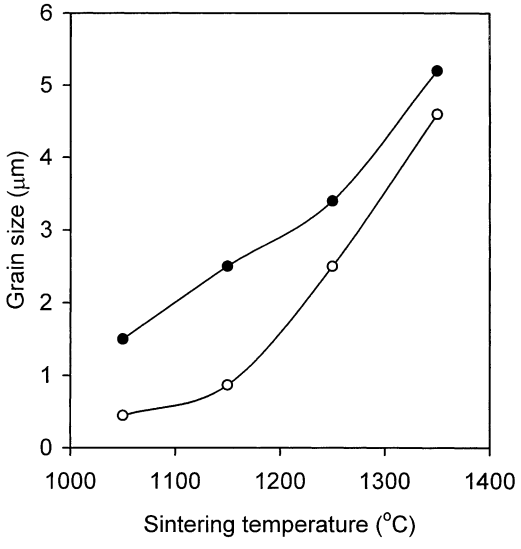

Fig. 6. The variation of grain sizes vs sintering temperature for the sample with Fe/Ce = 15% (● α-Fe_2O_3 and ○ CeO_2).

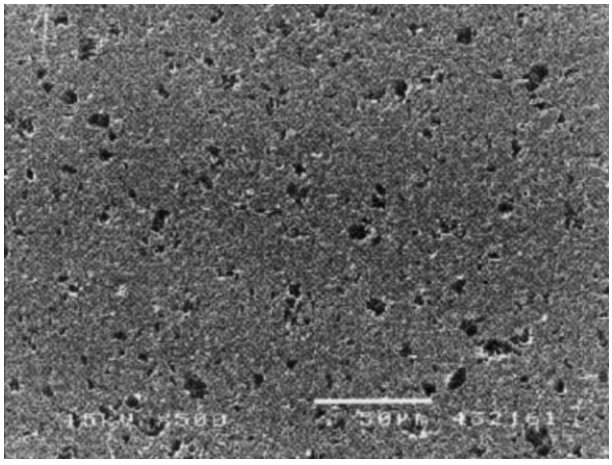

Fig. 7. SEM micrographs of the sample with Fe/Ce = 15% sintered for 5 h at (a) 1050°C and (b) 1350°C (dark grains are α-Fe_2O_3).

The variation in sintered densities (at 1050 and 1350°C) of the samples exhibits the similar trend. The sintered densities increases rapidly upon the addition of Fe_2O_3, and reach a maximum at ~0.5% Fe doping, then decreases with increasing Fe content. It seems that a higher Fe content decreases the density of the samples. We should note, however, that the samples with Fe/Ce ⩾ 1% can be treated as a two-phase composite. So the theoretical density of samples should change with the compositions due to the difference in both theoretical densities. For this case, the relative density of samples with different Fe contents can not be calculated using the theoretical density of pure CeO_2 for reference. The theoretical density for each composition can be calculated as follows:

$$\rho_s = \rho_c V_c + \rho_F V_F \quad (2)$$

and

$$V_c + V_F = 1 \quad (3)$$

where ρ_s, ρ_c and ρ_F are the theoretical densities of samples, CeO_2 and Fe_2O_3, respectively, V_c and V_F are the volume fractions of CeO_2 and Fe_2O_3. Supposing the solubility of Fe into CeO_2 is ~0.5% below 1350°C, which is reasonable based on XRD measurement and SEM observation.[14,15] According to formula (2), we obtain the theoretical density (ρ_s) for each composition. The relative density for each composition can be calculated using ρ_s for reference and is shown in Fig. 8. This figure clearly shows that the relative density keeps almost unchanged as Fe content increases in the range of 1–20%, for both the sintering temperatures. It means that below 1400°C, the densification of the samples with a large amount of Fe_2O_3 does not deteriorate.

The influence of Fe content on grain size at 1350°C is shown in Fig. 9. A rapid increase in grain size occurs in

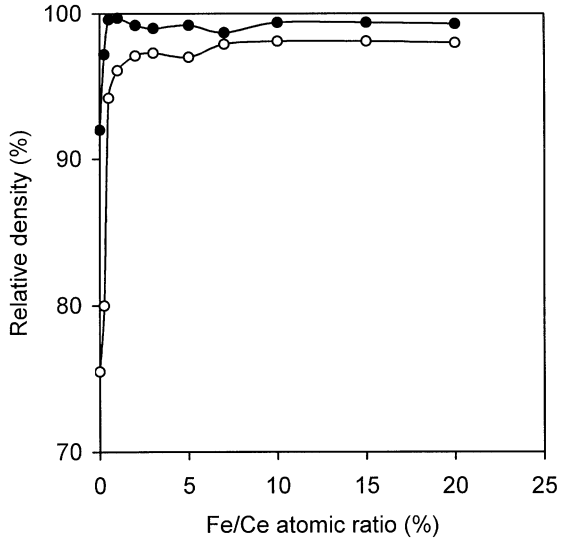

Fig. 8. Dependence of Fe/Ce atomic ratio (%) on the relative density of samples sintered at (○) 1050°C and (●) 1350°C for 5 h in air.

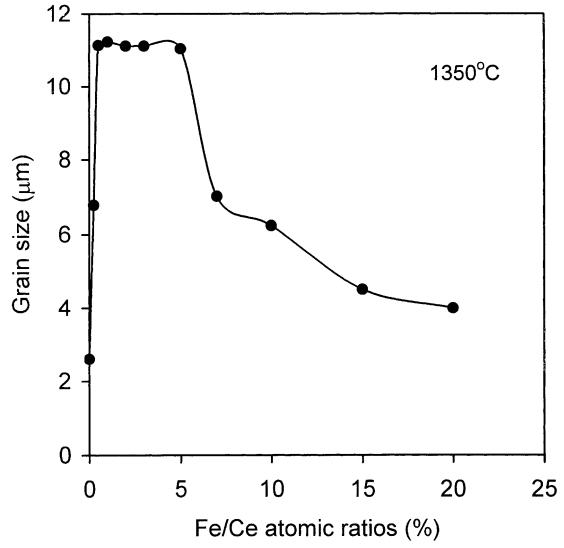

Fig. 9. Dependence of Fe/Ce atomic ratio (%) on grain size of samples sintered at 1350°C for 5 h in air.

the range of 0–0.5% Fe doping level. The grain size has then little change up to Fe/Ce = 5%. Subsequently a rapid decrease in grain size takes place in the 5–7% Fe content region, finally, grain size becomes smaller and smaller with increasing Fe content. As above-mentioned, the samples with Fe/Ce $\geqslant$ 1% are a two-phase composite. In a two-phase ceramic, second-phase particles have been used to inhibit grain growth and produce a fine-grain composite. Various studies have shown the grain growth of both phases in the zirconia-alumina system is significantly reduced.[22,23] The existing models[24–26] for explaining the pinning effect of second phase (β) on matrix phase (α) have been built up, supposing the grain size of second phase (β) kept unchanged, to study the grain growth of matrix. For example, Smith and Zener[24] predicted that a pinned growth state occurs at $D/r \propto 1/f$, where D is the diameter of the matrix grain, r is the radius of the pining particles and f is the volume fraction of pinning particles present.

No grain growth of second-phase particle coarsening models, however, has been set up to study a simultaneously coarsening of α and β phases. In our case, grain size of matrix (CeO_2) and pinning phase (Fe_2O_3) grows simultaneously, i.e. small D/r ratios. The increase in both the number and size of Fe_2O_3 grains do not affect the grain growth of CeO_2 in Fe content range of 1–5%. So-called pinning effect of second phase starts to take effect in the samples with Fe/Ce > 5%. At the present stage, a detailed explanation on this situation is not available.

4. Conclusions

A small amount of Fe doping significantly promotes the densification and grain growth of CeO_2 ceramic. 0.5% Fe-doped CeO_2 sintered at 1300°C for less than 1 h has ~99.2% R.D. (~6.4 μm in grain size), while undoped CeO_2 sintered under the same conditions has ~82.6% R.D. (~0.6 μm in grain size). The samples with Fe/Ce $\leqslant$ 1% exhibit a rapid grain growth above 1300°C. For pure CeO_2, however, a rapid grain growth occurs above 1500°C. It is assumed that different early-stage sintering mechanisms and the effect of severely undersized dopants are responsible for such these big differences in undoped and Fe-doped CeO_2.

Although so-called pining effect of second phase starts to take effect in the samples with Fe/Ce > 5%, the densification of the samples with Fe content ranging from 1 to 20% does not deteriorate when the sintering temperature is less than 1400°C. For the samples with Fe/Ce $\geqslant$ 1%, above 1400°C the densification behavior deteriorates remarkably; the density decreases with increasing sintering temperatures due to the appearance of lots of microcracks along grain boundaries.

References

1. Chawla, K. K., *Ceramic Matrix Composites*. Chapman & Hall, London, 1993.
2. Fang, D. W., Xu, T. and Qing, D. H., Positive temperature coefficient of resistance effect in hot-pressed cristobalite-silicon carbide composites. *J. Mater. Sci.*, 1994, **29**, 1097–1100.
3. Drofenik, M., Lisjak, D. and Zajc, I., Origin of the positive temperature coefficient of resistive anomaly in the ZnO–NiO system. *J. Am. Ceram. Soc.*, 1997, **80**, 1741–1748.
4. Lisjak, D., Zajc, I, Drofenik, M. and Jamnik, J., Investigation of the PTCR effect in ZnO–NiO two-phase ceramics. *Solid State Ionics*, 1997, **99**, 125–135.
5. Park, Y. M. and Choi, G. M., Microstructure and electrical properties of YSZ–NiO composites. *Solid State Ionics*, 1999, **120**, 265–274.

6. Kim, J. H. and Choi, G. M., Mixed ionic and electronic conductivity of $(ZrO_2)_{0.92}(Y_2O_3)_{0.081-y}(MnO_{1.5})_y$. *Solid State Ionics*, 2000, **130**, 157–168.
7. Panhans, M. A. and Blumenthal, R. N., A thermodynamic and electrical conductivity study of nonstoichiometric cerium dioxide. *Solid State Ionics*, 1993, **60**(4), 279–298.
8. Zhen, Y. S., Milne, S. J. and Brook, R. J., Oxygen ion conduction in CeO_2 ceramics simultaneously doped with Gd_2O_3 and Y_2O_3. *Sci. Ceram.*, 1988, **14**, 1025–1030.
9. Chen, P.-L. and Chen, I.-W., Reactive cerium (IV) oxide powders by the homogeneous precipitation method. *J. Am. Ceram. Soc.*, 1993, **76**(6), 1577–1583.
10. Chen, C. C., Nasrallah, M. M. and Anderson, H. U., Synthesis and characterization of $(CeO_2)_{0.8}(SmO_{1.5})_{0.2}$ thin films from polymeric precursors. *J. Electrochem. Soc.*, 1993, **140**(12), 3555–3560.
11. Zhu, Y. C. and Rahaman, M. N., Hydrothermal synthesis and sintering of ultrafine CeO_2 powders. *J. Mater. Res.*, 1993, **8**(7), 1680–1686.
12. Guillpu, N., Nistor, L. C., Fuess, H. and Haha, H., Microstructure study of nanocrystalline CeO_2 produced by gas condensation. *Nanostructural Mater.*, 1997, **8**(5), 545–557.
13. Chen, P.-L. and Chen, I.-W., Grain growth in CeO_2: dopant effects, defect mechanism, and solute drag. *J. Am. Ceram. Soc.*, 1996, **79**(7), 1793–1800.
14. Zhang, T., Peter, H., Huang, H. and Kilner, J., *J. Mater. Proc. Technol.*, in press.
15. Hrovat, M., Holc, J., Bernik, S. and Makorec, D., Subsolidus phase equilibria in the NiO–CeO_2 and La_2O_3–CeO_2–Fe_2O_3 systems. *Mater. Res. Bull.*, 1998, **38**(8), 1175–1183.
16. Wang, J. and Raj, R., Estimate of the activation energies for boundary diffusion from rate-controlled sintering of pure alumina doped with zirconia or titania. *J. Am. Ceram. Soc.*, 1990, **73**(5), 1172–1175.
17. Menddson, M. I., Average grain size in polycrystalline ceramics. *J. Am. Ceram. Soc.*, 1968, **52**(8), 443–446.
18. Zhou, Y. and Rahaman, M. N., Effect of redox reaction on the sintering behavior of cerium oxide. *Acta. Mater.*, 1997, **45**(9), 3635–3639.
19. Zhang, T., Peter, H., Huang, H. and Kilner, J., Submitted to *J. Mater. Sci.*
20. Bonnet, J. P., Dolet, N. and Heintz, J. M., Low-temperature sintering of 0.99 SnO_2–0.01 CuO: influence of copper surface diffusion. *J. Eur. Ceram. Soc.*, 1996, **16**, 1163–1169.
21. Gouvea, D., Varela, J. A. and Smith, J. P., Morphological characteristics of SnO_2 based powders containing manganess. *Eur. J. Solid State Inorg. Chem.*, 1996, **33**, 343–354.
22. French, J. D., Harmer, M. P., Chan, H. M. and Miller, G. A., Coarsening-resistant dual-phase interpenetrating microstructures. *J. Am. Ceram. Soc.*, 1990, **73**(8), 2508–2510.
23. Green, D. J., Critical microstructures for microcracking in Al_2O_3–ZrO_2 composites. *J. Am. Ceram. Soc.*, 1982, **65**(12), 610–614.
24. Smith, C. S., Grains, phases and interfaces: an interpretation of microstructure. *Trans. AIME*, 1948, **175**, 15–51.
25. Hillert, M., Inhibition of grain growth by second-phase particles. *Acta Metall.*, 1988, **36**(12), 3177–3181.
26. Hellman, P. and Hillert, M., On the effect of second-phase particles on grain growth. *Scand. J. Metall.*, 1975, **4**, 211.